

RESEARCH ARTICLE

Crystal Structure and Pyridoxal 5-Phosphate Binding Property of Lysine Decarboxylase from *Selenomonas ruminantium*

Hye-Young Sagong¹, Hyeoncheol Francis Son¹, Sunghwan Kim², Yong-Hwan Kim³, Il-Kwon Kim⁴, Kyung-Jin Kim^{1*}

1 School of Life Sciences, KNU Creative BioResearch Group, Kyungpook National University, Daegu, 702–701, Republic of Korea, **2** New Drug Development Center, Daegu-Gyungpook Medical Innovation Foundation, Daegu, 701–310, Republic of Korea, **3** School of Nano-Bioscience and Chemical Engineering, Ulsan National Institute of Science and Technology (UNIST), Ulsan, 689–798, Republic of Korea, **4** Bioprocess Research Depart. R&D Center, DAESANG Corp., Icheon-si, Gyeonggi-do, 17384, Republic of Korea

* kkim@knu.ac.kr



OPEN ACCESS

Citation: Sagong H-Y, Son HF, Kim S, Kim Y-H, Kim I-K, Kim K-J (2016) Crystal Structure and Pyridoxal 5-Phosphate Binding Property of Lysine Decarboxylase from *Selenomonas ruminantium*. PLoS ONE 11(11): e0166667. doi:10.1371/journal.pone.0166667

Editor: Eugene A. Permyakov, Russian Academy of Medical Sciences, RUSSIAN FEDERATION

Received: September 25, 2016

Accepted: November 1, 2016

Published: November 18, 2016

Copyright: © 2016 Sagong et al. This is an open access article distributed under the terms of the [Creative Commons Attribution License](https://creativecommons.org/licenses/by/4.0/), which permits unrestricted use, distribution, and reproduction in any medium, provided the original author and source are credited.

Data Availability Statement: All relevant data are within the paper and its Supporting Information files.

Funding: This work was supported by a National Research Foundation of Korea (NRF) grant (NRF-2014M1A2A2033626) and by C1 Gas Refinery Program through the National Research Foundation of Korea (NRF) funded by the Ministry of Science, ICT & Future Planning (NRF-2016M3D3A1A01913269), and was also supported by the New & Renewable Energy Core Technology Program of the Korea Institute of

Abstract

Lysine decarboxylase (LDC) is a crucial enzyme for acid stress resistance and is also utilized for the biosynthesis of cadaverine, a promising building block for bio-based polyamides. We determined the crystal structure of LDC from *Selenomonas ruminantium* (SrLDC). SrLDC functions as a dimer and each monomer consists of two distinct domains; a PLP-binding barrel domain and a sheet domain. We also determined the structure of SrLDC in complex with PLP and cadaverine and elucidated the binding mode of cofactor and substrate. Interestingly, compared with the apo-form of SrLDC, the SrLDC in complex with PLP and cadaverine showed a remarkable structural change at the PLP binding site. The PLP binding site of SrLDC contains the highly flexible loops with high b-factors and showed an open-closed conformational change upon the binding of PLP. In fact, SrLDC showed no LDC activity without PLP supplement, and we suggest that highly flexible PLP binding site results in low PLP affinity of SrLDC. In addition, other structurally homologous enzymes also contain the flexible PLP binding site, which indicates that high flexibility at the PLP binding site and low PLP affinity seems to be a common feature of these enzyme family.

Introduction

Two distinct types of bacterial amino acid decarboxylases have been reported [1]. Biodegradative enzymes such as L-histidine, L-glutamate, and L-lysine decarboxylase are highly induced at low pH and contribute to pH homeostasis [2]. The proton-dependent decarboxylation reaction increases the pH of the growth medium and is used as a defense mechanism against acid stress [3–7]. Biosynthetic enzymes are constitutively expressed regardless of pH variation and include L-ornithine, L-arginine, and L-lysine decarboxylases. These enzymes are responsible for the synthesis of polyamines such as putrescine, spermidine, and cadaverine, and are implicated

Energy Technology Evaluation and Planning (KETEP) granted financial resource from the Ministry of Trade, Industry & Energy, Republic of Korea (20153030091360).

Competing Interests: The authors have declared that no competing interests exist.

in a variety of cellular processes [8–10]. In particular, L-lysine decarboxylase (LDC) is an important enzyme for the biosynthesis of cadaverine, which is a crucial platform chemical with many industrial applications.

Cadaverine, also known as 1,5-diaminopentane, is an attractive chemical as a component of polymers such as polyamides and polyurethane [11]. Polyamides have been produced from petrochemicals and are used in a variety of commercial applications. In 2012, the global market was close to USD 22 billion and is estimated to reach USD 27 billion by 2018 [12]. Due to a growing interest in environment-friendly and sustainable resources, it is essential to produce industrially useful chemicals and materials from renewable resources. Bio-based polyamides are good alternatives to previous petrochemical routes in both environmental and economic aspects [13, 14]. Bio-based cadaverine can be obtained from the decarboxylation of L-lysine using LDC, and enzymatic production using external addition of LDC in lysine-rich medium has been proposed [15, 16].

The most attractive approach for a bio-based supply of cadaverine is microbial production using genetically engineered microorganisms such as *Escherichia coli* and *Corynebacterium glutamicum* [17, 18]. Systems metabolic engineering of these strains leads to an improved bio-synthetic capacity and a higher cadaverine yield [18–21]. However, two unsolved problems remain in the cadaverine production process. First, as one proton is consumed by the reaction, the pH of the medium increases [22]. Higher pH tends to decrease enzymatic activity, which in turn reduces cadaverine yield. Development of an LDC enzyme that preserves enzymatic activity at high pH is therefore necessary for effective cadaverine production. Second, cadaverine production requires continuous addition of pyridoxal-5-phosphate (PLP) as a cofactor due to the insufficiency of PLP for high level of LDC activity [19]. It has been reported that cadaverine yield increases with the addition of PLP in the medium. In addition, an *in vivo* supply of PLP was engineered, and the resulting additional supply of PLP led to a prolonged LDC reaction and thus to a higher final concentration of cadaverine [23].

In this report, we determined the crystal structures of LDC from *Selenomonas ruminantium* (SrLDC) in different crystallization conditions and observed that high flexibility of the PLP binding site seems to be one of the factors that lead to the low affinity for PLP in SrLDC. By comparing the SrLDC structure with other similar enzymes, the active site flexibility is a common structural feature in this enzyme family.

Materials and Methods

Production of SrLDC

The gene coding for lysine decarboxylase from *S. ruminantium* (SrLDC, amino acid residues 1–399) was amplified from chromosomal DNA of *S. ruminantium* by polymerase chain reaction (PCR) with primers: forward, 5-GCGCGCATATGAAAACTTCCGTTTAAGCGAA AAAG -3, and reverse, 5-GCGCGCTCGAGGTGATGGTGATGGTGGTGAAGTCT-3. The PCR product was then subcloned into the pET-22b(+) vector (Life Science Research) with 6x-histag at the C-terminus. The resulting expression vector pET-22b(+):*Srldc* was transformed into the *E. coli* strain BL21(DE3)-T1^R, which was grown in 1 L of LB medium containing 100 µg/mL ampicillin at 37°C until the OD 600 reached 0.7. After induction with 1.0 mM 1-thio-β-D-galactopyranoside (IPTG), the culture medium was maintained for a further 20 h at 18°C. The culture was then harvested by centrifugation at 4,000 × g for 20 min at 4°C. The cell pellet was resuspended in buffer A (40 mM Tris-HCl, pH 8.0) and disrupted by ultrasonication. The cell debris was removed by centrifugation at 13,500 × g for 30 min and the lysate was applied to a Ni-NTA agarose column (Qiagen). After washing with buffer A containing 30 mM imidazole, the bound proteins were eluted with 300 mM imidazole in buffer A. Finally,

trace amounts of contaminants were removed by size-exclusion chromatography using a Superdex 200 prep-grade column (320 mL, GE Healthcare) equilibrated with buffer A. All purification experiments were performed at 4°C. SDS-polyacrylamide gel electrophoresis analysis of the purified proteins showed a single polypeptide of 44.0 kDa that corresponded to the estimated molecular weight of the SrLDC monomer. The purified protein was concentrated to 65 mg mL⁻¹ in 40 mM Tris-HCl, pH 8.0.

Crystallization of SrLDC

Crystallization of the purified protein was initially performed with commercially available sparse-matrix screens from Rigaku and Molecular Dimensions by using the hanging-drop vapor-diffusion method at 20°C. Each experiment consisted of mixing 1.0 µL of protein solution (65 mg mL⁻¹ in 40 mM Tris-HCl, pH 8.0) with 1.0 µL of reservoir solution and equilibrating the drop against 0.5 mL of reservoir solution. The apo-form I crystals of SrLDC were observed in several crystallization screening conditions. After several optimization steps, the best quality crystals appeared in 4 days using a reservoir solution consisting of 28% (w/v) polyethylene glycol (PEG) 400, 0.1 M sodium citrate tribasic-citric acid, pH 6.0, and 0.2 M magnesium chloride at 20°C. The apo-form II crystals of SrLDC were crystallized in the condition containing 1.15 M sodium citrate and 0.1 M sodium cacodylate, pH 5.0. The crystals of SrLDC complexed with PLP/cadaverine were crystallized in the condition of 50% PEG 200, 0.1 M sodium phosphate, pH 4.2, 0.2 M sodium chloride, and 5 mM PLP. We then soaked 10 mM L-lysine into the crystals for 30 min.

Data collection and structure determination of SrLDC

The crystals were transferred to a cryo-protectant solution composed of the corresponding condition described above and 30% (v/v) glycerol, fished out with a loop larger than the crystals, and flash-frozen by immersion in liquid nitrogen. All data were collected at the 7A beam-line of the Pohang Accelerator Laboratory (PAL, Pohang, Korea), using a Quantum 270 CCD detector (ADSC, USA). The crystals of the apo-forms I and II of SrLDC diffracted to 2.0 and 2.9 Å resolutions, respectively. The crystals of SrLDC complexed with PLP/cadaverine crystals diffracted to 2.5 Å resolutions. All data were indexed, integrated, and scaled using the HKL-2000 software package [24]. The apo-form I crystals of SrLDC belonged to the space group $P4_32_12$ with unit cell parameters $a = b = 105.97$ Å, $c = 73.634$ Å, $\alpha = \beta = \gamma = 90.0^\circ$. With one molecule of SrLDC per asymmetric unit, the crystal volume per unit of protein mass was 2.35 Å³ Da⁻¹, indicating that the solvent content was approximately 47.63% [25]. The apo-form II of SrLDC crystals belonged to the space group C2 with unit cell dimensions of $a = 146.45$ Å, $b = 70.794$ Å, $c = 88.061$ Å, $\alpha = \gamma = 90.0^\circ$, $\beta = 101.03^\circ$. With two molecules per asymmetric unit, the crystal volume per unit of protein mass was 2.54 Å³ Da⁻¹, which corresponds to a solvent content of 51.68% [25]. The PLP/cadaverine-complexed form of SrLDC crystals belonged to the space group $P6_32_2$ with unit cell dimensions of $a = b = 111.73$ Å, $c = 112.97$ Å, $\alpha = \beta = 90.0^\circ$, $\gamma = 120.0^\circ$. With one molecule per asymmetric unit, the crystal volume per unit of protein mass was 2.31 Å³ Da⁻¹, and the solvent content was 46.83% [25]. The structure of the apo-form I of SrLDC was solved by molecular replacement with the CCP4 version of MOLREP [26] using the structure of L/ODC from *Vibrio vulnificus* (VvL/ODC, PDB code 2PLK) as a search model. Model building was performed manually using the program WinCoot [27] and refinement was performed with CCP4 refmac5 [28]. The structures of the apo-form II of SrLDC, SrLDC complexed with PLP/cadaverine were determined by molecular replacement using the refined SrLDC structure of apo-form I. Model building and structure refinement of these structures were performed using a procedure similar to that employed for the structure

of the apo-form I of SrLDC. Data collection and refinement statistics are summarized in Table 1. Four refined SrLDC structures of apo-form I, apo-form II, and complexed with PLP/cadaverine were deposited in the Protein Data Bank with PDB codes of 5GJN, 5GJM, and 5GJP, respectively.

LDC activity assay

To measure the lysine decarboxylase (LDC) activity of the SrLDC proteins, 56.78 μM of purified enzyme was added to 200 μl of reaction mixture containing 0.1 M potassium phosphate, pH 6.0, 50 μM L-lysine, and various concentrations of PLP. The reaction mixtures were incubated at 37°C for 30 sec. The reaction was stopped by heating the solution at 90°C for 5 min. After centrifugation at 13,500 × g for 5 min, the remaining L-lysine was detected using the lysine oxidase/peroxidase method. Lysine oxidase converts the remaining L-lysine into

Table 1. Data collection and structural refinement statistics of SrLDC.

	SrLDC		
	Apo I 5GJN	Apo II 5GJM	+ PLP/cadaverine 5GJP
Data collection			
Space group	<i>P4₃2₁2</i>	<i>C2</i>	<i>P6₃2₂</i>
Cell dimensions			
<i>a, b, c</i> (Å)	106.0, 106.0, 73.6	146.5, 70.8, 88.1	111.7, 111.7, 113.0
α, β, γ (°)	90.0, 90.0, 90.0	90.0, 101.0, 90.0	90.0, 90.0, 120.0
Resolution (Å)	50.0–2.0 (2.03–2.0)*	50.0–2.9 (2.95–2.9)*	50.0–2.5 (2.54–2.5)*
<i>R</i> _{sym} or <i>R</i> _{merge}	7.3 (30.4)	14.5 (34.6)	13.2 (31.7)
<i>I</i> / <i>σ</i> <i>I</i>	61.0 (10.0)	23.9 (8.5)	89.7 (11.4)
Completeness (%)	99.1 (100.0)	95.2 (94.2)	96.8 (95.1)
Redundancy	11.1 (10.8)	3.5 (3.3)	24.2 (12.9)
Refinement			
Resolution (Å)	50.0–2.0	50.0–2.9	50.0–2.5
No. reflections	27192	17748	13670
<i>R</i> _{work} / <i>R</i> _{free}	20.3/24.0	17.7/23.2	19.8/27.9
No. atoms	3107	5913	3034
Protein	2854	5785	2948
Ligand/ion	40	6	48
Water	213	122	38
<i>B</i> -factors	44.4	21.2	52.0
Protein	31.7	21.4	51.2
Ligand/ion	59.9	38.7	65.8
Water	48.6	13.1	50.1
B from Wilson plot (Å ²)	37.5	21.8	43.1
R.m.s. deviations			
Bond lengths (Å)	0.019	0.019	0.019
Bond angles (°)	1.921	1.704	1.636
Ramachandran statistics (%)			
Favored	97.5	97.2	98.6
Allowed	2.5	2.8	1.3
Outliers	0.0	0.0	0.0

*The numbers in parentheses are statistics from the highest resolution shell.

doi:10.1371/journal.pone.0166667.t001

6-amino-2-oxohexanoate, NH_3 , and H_2O_2 , and the H_2O_2 is then reduced by peroxidase using 2,2'-azino-bis(3-ethylbenzothiazoline-6-sulphonic acid) (ABTS). After the LDC reaction, equal volume of 2x lysine oxidase/peroxidase solution (0.1 unit ml^{-1} lysine oxidase, 1 unit ml^{-1} peroxidase, and 3.6 mM ABTS in 0.1 M potassium phosphate buffer, pH 8.0) was added to the LDC reaction mixture. The amount of oxidized ABTS was detected by measuring absorbance at 412 nm. All experiments were performed in triplicate.

Isothermal titration calorimetry

The binding affinity between SrLDC and PLP was measured using a Nano ITC model (TA Instruments) at 20°C. Protein sample at 100 μM was prepared in 40 mM Tris, pH 8.0. For titrations of SrLDC with PLP, 1.96 μl of 2.5 mM PLP was injected 25 times. Each injection was monitored at 200-second intervals and the protein solution in the ITC reaction cell was stirred at 250 RPM. The heat of cofactor dilution into the buffer was subtracted from the reaction heat. Calculated heat area per injection was used for fitting in the independent binding model for calculation of the thermodynamic parameter (K_d).

Results and Discussion

Overall structure of SrLDC

To reveal the molecular mechanism of SrLDC, we determined its crystal structure at 2.0 Å resolution (Table 1). The asymmetric unit contains one SrLDC molecule, and the dimeric structure of the protein could be easily generated by applying crystallographic $P4_32_12$ symmetry. SrLDC shows an overall fold similar to that of other constitutively expressed ornithine decarboxylases such as *Vibrio vulnificus* lysine/ornithine decarboxylase (VvL/ODC, PDB code 2PLK), *Mus musculus* ODC (MmODC, PDB code 7ODC), and *Trypanosoma brucei* ODC (TbODC, PDB code 1F3T) (Fig 1A). The monomeric form of SrLDC consists of two distinct domains, a PLP-binding barrel domain, and a sheet domain. The barrel domain (Leu27-Cys261) is composed of eight α -helices ($\alpha 2$ - $\alpha 9$) and eight parallel β -strands ($\beta 2$ - $\beta 9$) in an alternating pattern (Fig 1B). The eight α -helices wrap the eight-stranded β -sheet core that serves as a cofactor binding site. The sheet domain (Met1-Ser26, Gly262-Val393) is formed by a seven-stranded anti-parallel β -sheet ($\beta 1$, $\beta 10$ - $\beta 15$) that is surrounded by three short α -helices (Fig 1B). This domain contributes mainly to dimerization. The SrLDC homodimer is formed by a head-to-tail contact between the barrel domain of one monomer and the sheet domain of the other monomer (Fig 1C). PISA software [29] calculated that a 2,474.4 Å² area of solvent-accessible interface per monomer is buried, and the percentage of participating residues is 19.7%. Two identical active sites lie at the dimer interface and both active sites contain residues from each monomer.

Cofactor and substrate binding mode of SrLDC

To understand the cofactor and substrate binding modes of SrLDC, we determined the crystal structure of this enzyme complexed with PLP and cadaverine at 2.5 Å resolution. Unlike the apo-form, the SrLDC structure complexed with PLP/cadaverine belongs to the $P6_32_2$ space group (Table 1). Although we soaked the crystals of SrLDC complexed with PLP in L-lysine, a cadaverine molecule was observed instead. We suspect that L-lysine was converted into cadaverine during the soaking process. The PLP cofactor binds mainly to the pocket formed at the barrel domain (Fig 2A), and the catalytic residue Lys51 interacts with the aldehyde group of the pyridoxal ring. The pyridine ring is stabilized by hydrogen bond between N1 of the ring and the acidic residue Glu255 (Fig 2B). The phosphate moiety of PLP is mainly stabilized by

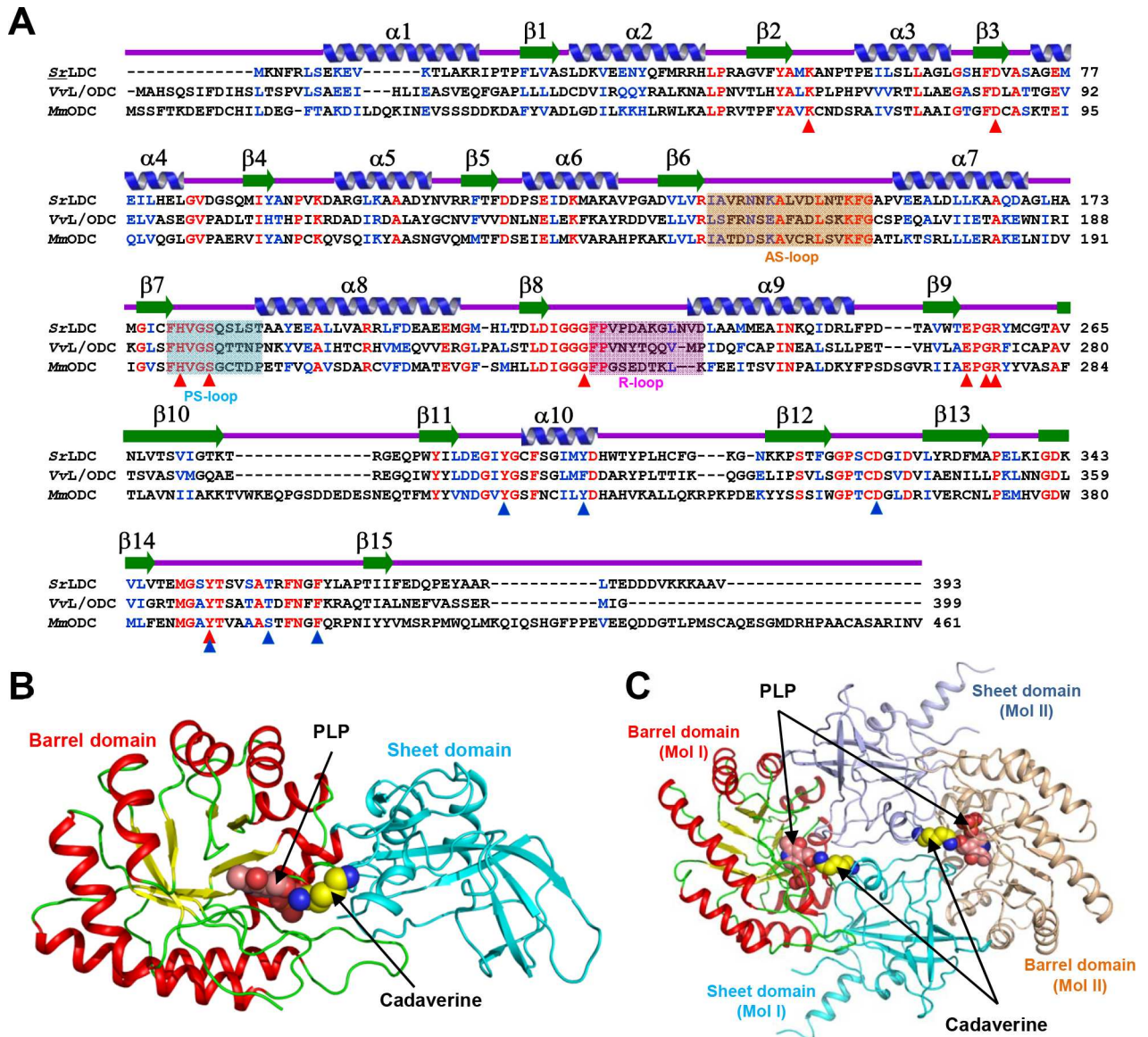


Fig 1. Crystal structure of *SrLDC*. (A) Amino acid sequence alignment of L/ODCs. Identical and highly conserved residues are presented red and blue colored characters, respectively. Secondary structure elements are drawn based on the *SrLDC* structure in an apo-form. The AS-loop, PS-loop and R-loop are shown in boxes with orange, cyan and magenta colors, respectively. Residues involved in binding of PLP and substrate are marked with red- and blue-colored triangles, respectively. *SrLDC*, *VvL/ODC*, and *MmODC* are representatives of lysine decarboxylase from *Selenomonas ruminantium*, lysine/ornithine decarboxylase from *Vibrio vulnificus*, and ornithine decarboxylase from *Mus musculus*, respectively. (B) Monomeric structure of *SrLDC*. A monomeric protein is shown as a cartoon diagram. The barrel domain is presented with colors of red and yellow for α -helices and β -strands, and the sheet domain is with a cyan color. The bound PLP and cadaverine are shown as sphere models with salmon and yellow colors, respectively. (C) Dimeric structure of *SrLDC*. The dimeric structure of *SrLDC* is shown as a cartoon diagram showing one monomer with a color scheme in (B) and the other monomer in light-orange and light-blue for the barrel domain and the sheet domain, respectively. The bound PLP and cadaverine are shown as sphere models with salmon and yellow colors, respectively.

doi:10.1371/journal.pone.0166667.g001

strong hydrogen bonds with the side-chains of His179, Ser182, and Tyr352, and the main-chains of Gly219, Gly257, and Arg258 are also involved in the stabilization of the moiety (Fig 2B). A shallow substrate-binding hole is formed at the interface between the sheet domains of two monomers (Fig 2A). The ϵ -amino group of the cadaverine product seems to be stabilized

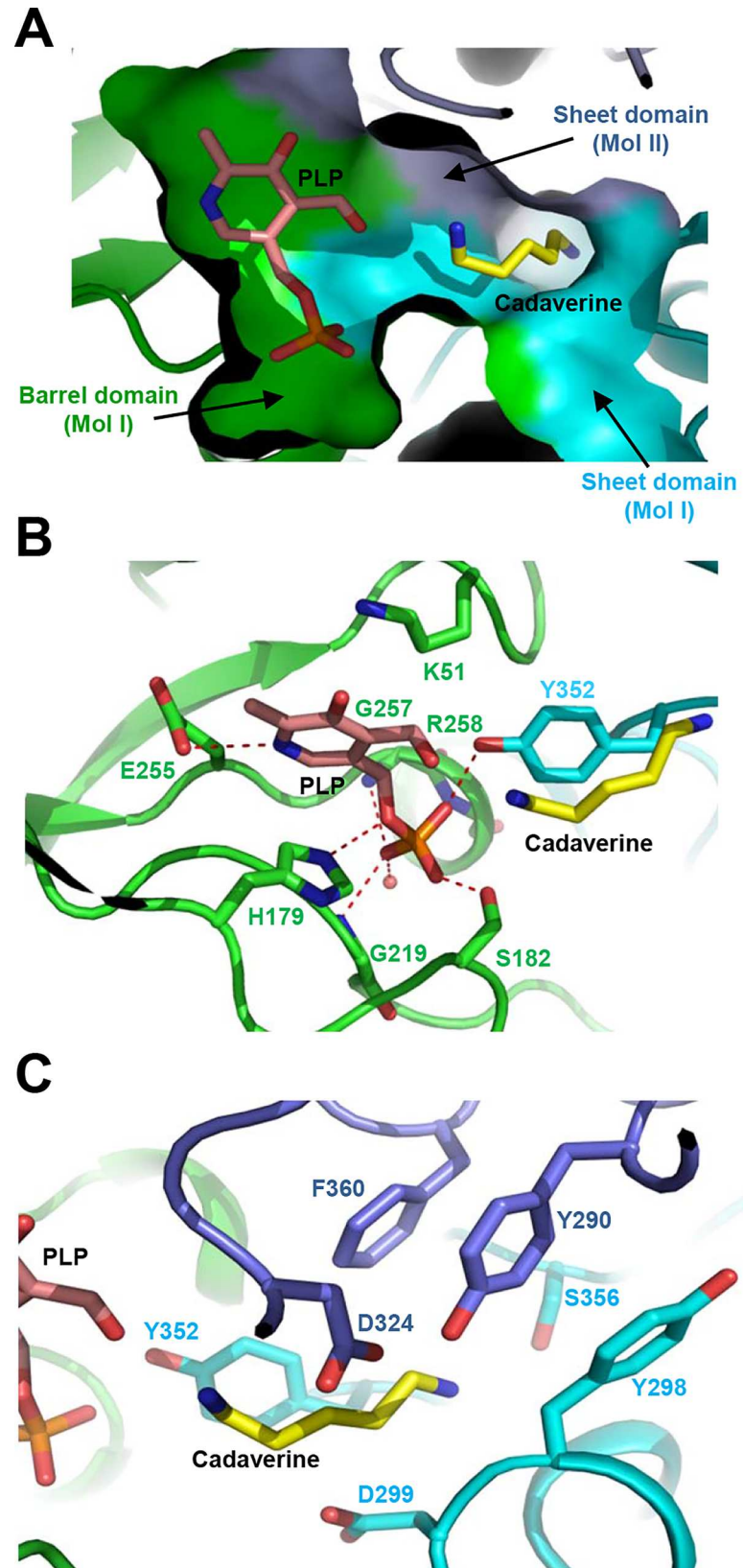


Fig 2. Cofactor and substrate binding mode of SrLDC. (A) A surface model of the active site of SrLDC. The SrLDC structure complexed with PLP/cadaverine is presented with a surface model with colors of green, cyan, and light-blue for the barrel domain and the sheet domain of one monomer and the sheet domain of the other monomer, respectively. The bound PLP and cadaverine are shown as stick models with salmon and yellow colors, respectively. (B) PLP binding mode of SrLDC. The SrLDC structure complexed with PLP/cadaverine is presented with a cartoon diagram with the same color scheme as in (A). The residues involved in the PLP binding are shown as stick models and labeled. The hydrogen bonds involved in the PLP binding are shown as red-colored dotted lines. The bound PLP and cadaverine are shown as stick models with salmon and yellow colors, respectively. (C) Substrate binding mode of SrLDC. The SrLDC structure complexed with PLP/cadaverine and residues involved in the substrate binding are presented as (B).

doi:10.1371/journal.pone.0166667.g002

by hydroxyl groups of residues Tyr290 and Ser356. Hydrophobic residues such as Tyr298 and Phe360 provide hydrophobicity for the stabilization of five methylene groups of cadaverine. Asp299 also aids the stabilization of hydrophobic parts of cadaverine. Residues Asp324 and Tyr352 are located in the vicinity of the α -amino group of cadaverine (Fig 2C).

High flexibility at the active site of SrLDC

Importantly, we observed a large conformational change in SrLDC upon binding of the PLP cofactor. When we superimpose the structure of the apo-form of SrLDC in $P4_32_12$ space group with that of SrLDC complexed with PLP/cadaverine, the overall shape of the two structures is almost the same, with an R.M.S.D. value of 0.72 Å. However, remarkable structural differences are observed at the active site (Fig 3A). Interestingly, in the structure of the apo-form of SrLDC, the connecting loop between β -7 and α -8 (Phe178-Thr187) moved away from the PLP binding site by a distance of 5.0 Å, compared with the structure of SrLDC complexed with PLP/cadaverine (Fig 3A). The loop is heavily involved in the stabilization of PLP by forming hydrogen bonds between residues His179 and Ser182 and the phosphate moiety of PLP (Fig 3A). Because the conformational change disrupts these hydrogen bonds between the loop and the phosphate moiety of PLP, it might severely impair binding of the cofactor to the protein. Hereafter, the loop will be referred to as a PLP stabilization loop (PS-loop). Also interestingly, the conformational change of the PS-loop subsequently causes a more dramatic conformational change in the loop connecting β -8 and α -9 (Phe220-Asp231). The loop, located near the PLP binding site in the structure of SrLDC complexed with PLP/cadaverine, moved away from the PLP binding site by a distance of 12.2 Å in the structure of the apo-form (Fig 3A). These structural observations clearly show that SrLDC has an open conformation in the apo-form and a closed conformation in the complexed form (Fig 3B and 3C). The stabilization modes of the loop are also quite different from each other. In SrLDC complexed with PLP/cadaverine, the main-chain of Phe220 forms a water-mediated hydrogen bond network with the main-chain of Tyr259 and phosphate moiety of PLP. The main-chain of Ala225 forms a direct hydrogen bond with the main-chain of Thr302. The loop also interacts with the PS-loop by a hydrogen bond between the side-chain of Q183 and the main-chain of Val222 (Fig 3D). In contrast, in the apo-form of SrLDC, the loop is stabilized by the N-terminal region instead: the main-chains of Met1 and Leu228 form a hydrogen bond with each other, and the main-chains of Pro223 and Ala225 form hydrogen bonds with both the side- and the main-chains of Asn3 (Fig 3E). The loop conformation seems to directly influence the PS-loop conformation, and we will refer to this loop as regulatory loop (R-loop). An additional loop worth mentioning is the one connecting β -6 and α -7 (Ile137-Gly153). This loop is known to be disordered or highly flexible in this family of enzymes, and to undergo conformational change controlling the substrate's access to the active site [30, 31]. The loop is also disordered both in the apo-form of SrLDC and in the form complexed with PLP/cadaverine (Fig 3A). Considering the function of the loop, we will refer to it as active site loop (AS-loop).

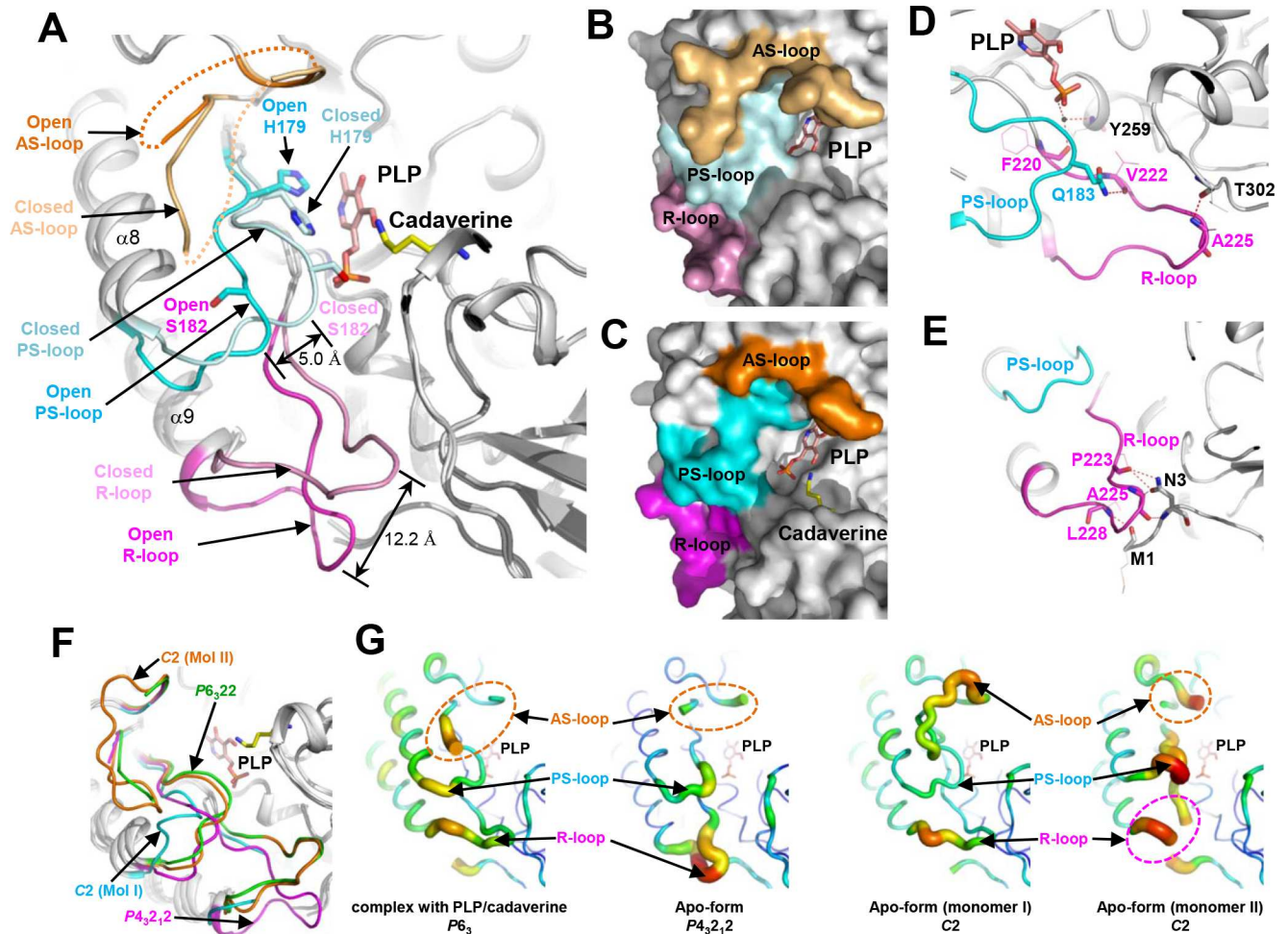


Fig 3. Highly flexible active site of *SrLDC*. (A) Open and closed conformational changes of the active site of *SrLDC*. The *SrLDC* structures in the apo-form and complexed with PLP/cadaverine are superimposed and presented with cartoon diagrams. The AS-loop, the PS-loop, and the R-loop in the open and closed conformations are distinguished with different colors and labeled. The bound PLP and cadaverine are shown as stick models with salmon and yellow colors, respectively. (B) (C) Surface models of the open and closed conformations. The AS-loop, the PS-loop, and the R-loop in the closed (B) and open (C) conformations are presented with surface models with the same color scheme as in (A). (D) (E) Stabilization mode of the PS-loop and the R-loop. The PS-loop and the R-loop in the closed (D) and open (E) conformations are presented with cartoon diagrams with the same color scheme as in (A). Side-chains involved in the stabilization of the PS-loop and the R-loop are shown as stick models. Main-chains involved in the stabilization of the PS-loop and the R-loop are shown as stick models and their side-chains are as line models. Hydrogen bonds are presented as red-colored dotted lines. (F) Superimposition of *SrLDC* structures in three different crystal forms. Four monomeric *SrLDC* structures in three different crystal forms are superimposed and presented as cartoon diagrams. The AS-loop, PS-loop, and the R-loop of four monomers are distinguished with different colors and labeled. (G) B-factor presentation of *SrLDC* structures in three different crystal forms. The crystal forms are labeled at the bottom of the figures. The AS-loop, PS-loop, and the R-loop are labeled.

doi:10.1371/journal.pone.0166667.g003

The observed conformational changes of the three loops, PS-, R-, and AS-loop, lead us to propose that *SrLDC* undergoes large open-closed conformational changes upon binding of the PLP cofactor and/or the lysine substrate. However, the space groups of the *SrLDC* structures in the apo-form ($P4_32_12$) and in the form complexed with PLP/cadaverine ($P6_32_2$) are different from each other (Table 1). Because different crystal packing can influence the local conformations of proteins, the question of whether the observed open-closed conformational changes are physiologically relevant remains. To investigate the conformational changes at the active site of *SrLDC*, we determined its crystal structure in the apo-form with a C2 space group at 2.9 Å resolution (Table 1). Unlike the two crystal forms described above, the structure contains a

dimer in an asymmetric unit. Interestingly, two *SrLDC* monomers in the asymmetric unit exhibit completely different conformations at the active site, although no cofactor or substrate is bound in either monomer. In one monomer, the PS-loop is in the open-conformation and the R-loop is disordered (Fig 3F). In contrast, the other monomer contains both the PS-loop and the R-loop in the closed-conformation observed in the structure of *SrLDC* complexed with PLP/cadaverine. Moreover, the entire AS-loop is in an ordered-conformation with a clear electron density map in this region (Fig 3F). These observations indicate that the open-closed conformation of *SrLDC* is caused mainly by the different crystal packings rather than by the binding of the PLP cofactor and/or the lysine substrate (S1 Fig). In fact, the PS-loop, the R-loop, and the AS-loop all show a much higher b-factor compared with the rest of the protein (Fig 3G), indicating that these loop regions are highly flexible. Taken together, the results allow us to conclude that the active site of *SrLDC* has an extremely high flexibility.

Low PLP affinity in *SrLDC*

As described above, *SrLDC* exhibits highly flexible active site. We then tested the PLP requirements of *SrLDC* by measuring the LDC activity of the recombinant protein in various concentrations of PLP. As expected, the recombinant *SrLDC* protein showed no noticeable activity in the reaction mixture without PLP supplement. When various concentrations of PLP were added to the reaction mixture, activity of the recombinant *SrLDC* was detected and reached its maximum at 0.1 mM or higher concentrations of PLP (Fig 4A). These results indicate that the PLP cofactor was detached from the recombinant *SrLDC* protein during the purification procedure, and the enzyme thus showed no activity without PLP supplement. To investigate if requirement of the additional PLP supplement for LDC activity is due to the low affinity of *SrLDC* for PLP, we measured the K_d value of the protein for PLP using isothermal titration calorimetry. The result showed that *SrLDC* has a somewhat high K_d value of 72 μM (Fig 4B and 4C). Interestingly, other PLP-dependent enzymes such as tryptophan synthase and tyrosine phenol lyase exhibited much higher PLP affinity than *SrLDC* with K_d values of 0.9 μM [32] and 2.0 μM [33]. Based on these results and the structural observations described above, we propose that highly flexible active site might contribute to the low affinity for the PLP cofactor in *SrLDC*.

Flexible active sites of other L/ODCs

We then investigated the active site flexibility of other structurally homologous enzymes. When we superimposed the *SrLDC* structure with the PLP-complexed structures of *VvL/ODC*, *MmODC*, and *TbODC*, the overall structures were quite similar to each other, with R.M.S.D. values of 1.2, 1.4, and 1.4 \AA , respectively. Although all three PLP-complexed L/ODC structures show closed conformations similar to that observed in the structure of *SrLDC* complexed with PLP/cadaverine, the PS-loop and R-loop conformations are somewhat different in each structure. The PS-loops of *MmL/ODC* and *TbODC* are positioned slightly away from the PLP binding site compared with that of *SrLDC* (Fig 5A). In the *MmODC* structure in particular, this conformational difference resulted in a water-mediated hydrogen bonding between Ser200 and the phosphate moiety instead of a direct hydrogen bond found in other proteins (S2 Fig). More pronounced differences were observed in R-loops. Although the R-loop of *VvL/ODC* shows a conformation quite similar to that of the closed form of *SrLDC*, the R-loops of *MmO/LDC* and *TbODC* are in an intermediate position between the open and the closed conformations of *SrLDC* (Fig 5A). Most importantly, the AS-, PS- and R-loops of these structures exhibit a high b-factor, similar to those observed in *SrLDC* (Fig 5B, 5C and 5D). One exception is *VvL/ODC*, which shows a relatively low b-factor compared to other structures, however, this

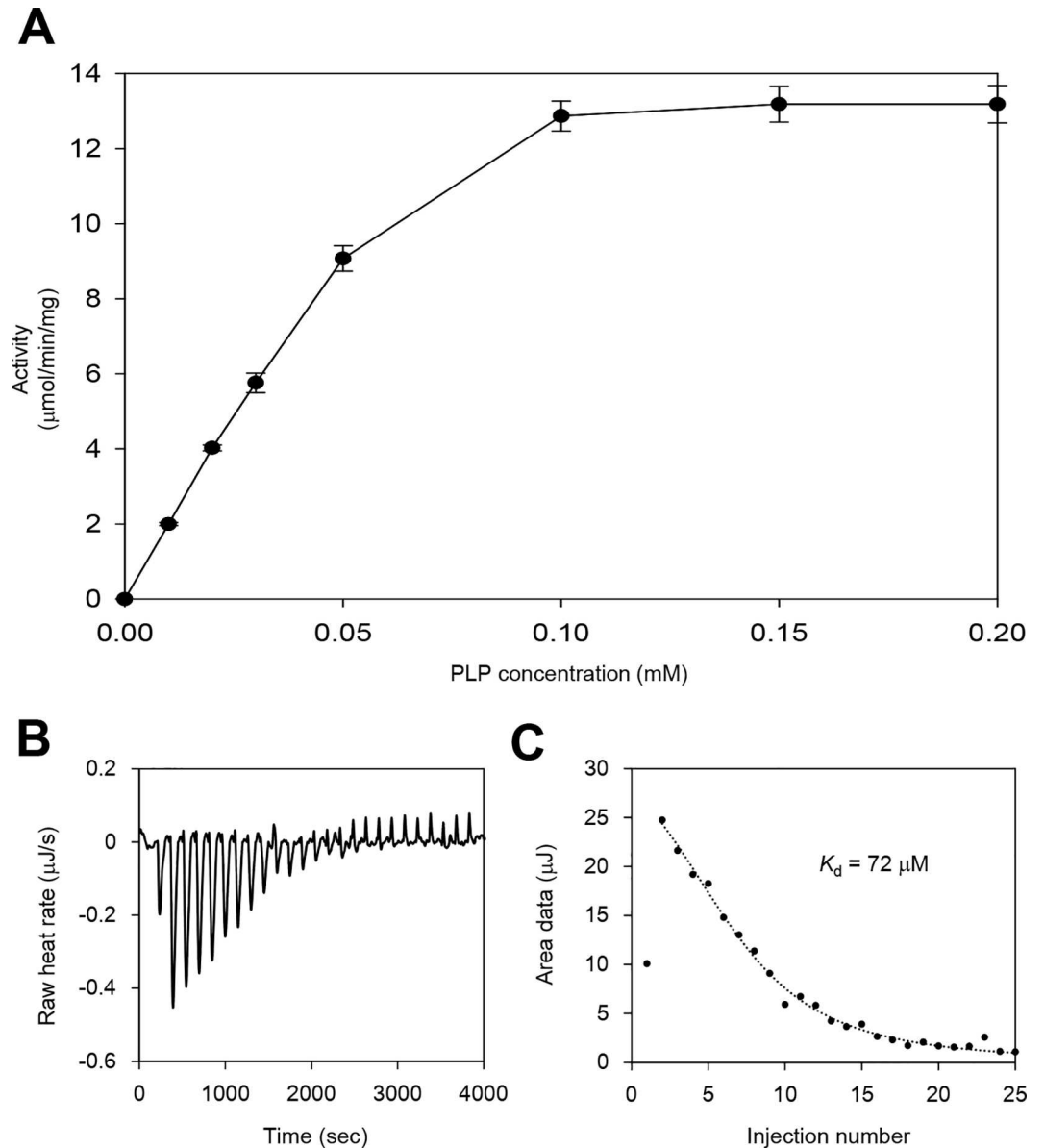


Fig 4. LDC Activity of SrLDC. (A) LDC activity of SrLDC at various concentrations of PLP. LDC activity of SrLDC was measured with various concentrations of PLP (0, 0.01, 0.02, 0.03, 0.05, 0.1, 0.15, and 0.2 mM). All experiments were performed in triplicates. (B) (C) Raw (B) and fitted (C) data of Isothermal titration calorimetry of SrLDC. The binding interactions between SrLDC and PLP were carried out using isothermal titration calorimetry (Nano ITC model, TA Instruments).

doi:10.1371/journal.pone.0166667.g004

difference seems to be derived from the tight crystal packing of the structure (S3 Fig). In addition, it has been reported that PLP was added to the reaction mixture during the enzymatic activity assays of these enzymes. Based on these results, we suggest that a flexible active site is not confined only to SrLDC, but rather is a common structural feature of this enzyme family.

Conclusion

PLP is a versatile cofactor and is utilized in a variety of reactions [34]. In particular, PLP-dependent enzymes are involved in the production of amino acids and amine-containing

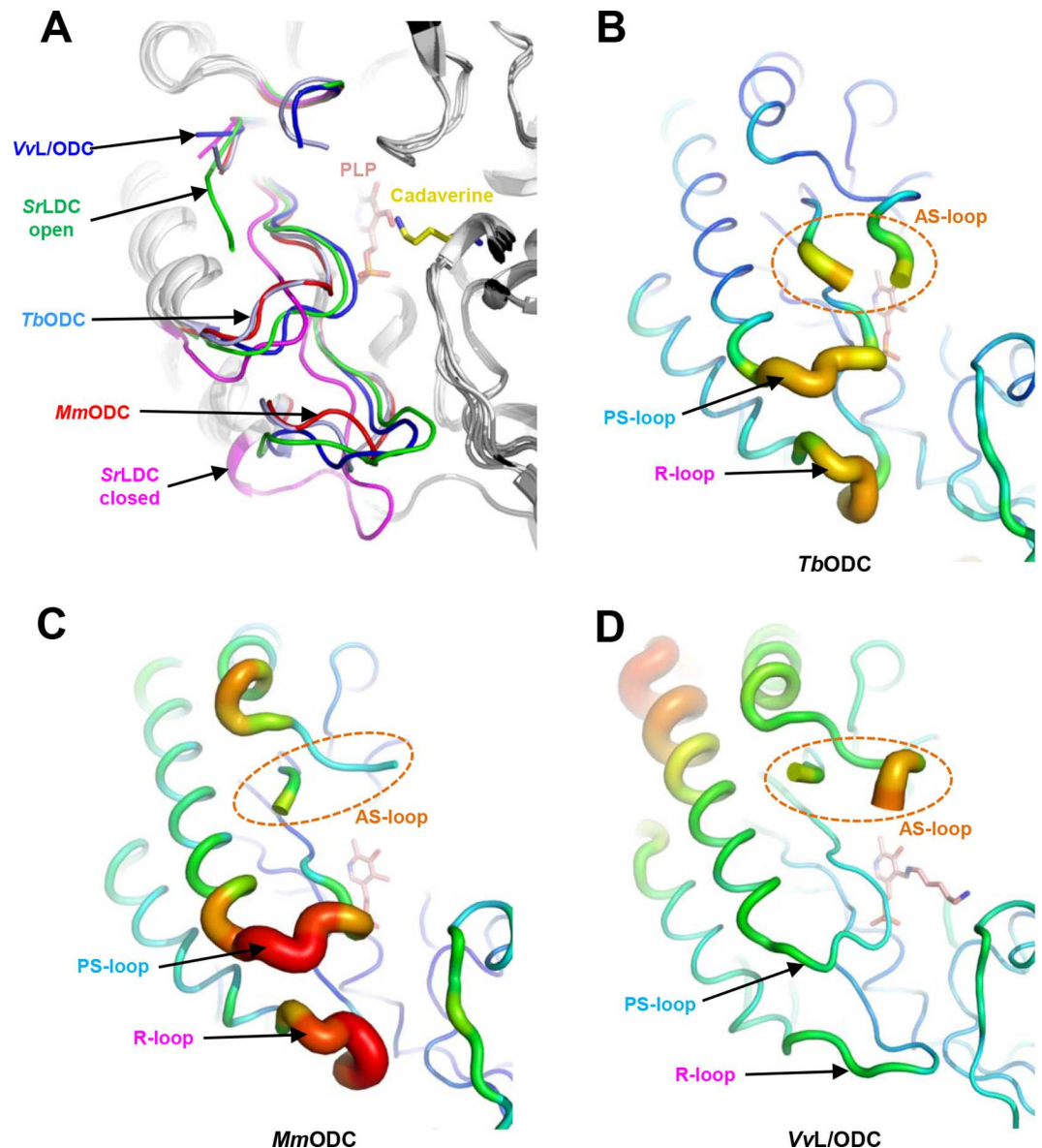


Fig 5. Flexible active sites of other L/ODCs. (A) Superimposition of L/ODC structures. Structures of the open and closed conformations of *SrLDC* and those of *TbODC*, *MmODC*, and *VvL/ODC* are superimposed. The AS-loop, PS-loop and the R-loop of these structures are distinguished with different colors and labeled. (B) (C) (D) B-factor presentation of the structures of *TbODC* (B), *MmODC* (C), and *VvL/ODC* (D). The AS-loop, PS-loop and the R-loop of these structures are labeled.

doi:10.1371/journal.pone.0166667.g005

compounds by means of their decarboxylation and transamination activities. However, due to the low PLP binding affinity, several PLP-dependent enzymes require additional supplements of PLP to maintain their activities [35]. For this reason, PLP has been one of the critical control factors for the production of industrially important materials. Many attempts have been also made to minimize the additional cost of a continuous supply of PLP in the production of cadaverine. Recently, a *de novo* PLP biosynthetic pathway was introduced into the cadaverine-producing strains to increase the cellular level of PLP [23]. The structural studies in this report provides structural basis for low PLP affinity of LDCs, and might be utilized for future protein engineering to enhance the affinity for PLP in this family enzymes.

Supporting Information

S1 Fig. Different contacts of SrLDC with neighboring molecules in different crystal forms. One SrLDC structure is shown as a cartoon diagram. The AS-loop, PS-loop and the R-loop of SrLDC are colored orange, cyan, and magenta, respectively. The molecules near SrLDC are shown as surface models with different colors.

(TIF)

S2 Fig. Mode of hydrogen bonding between a serine residue on the PS-loop and PLP. The Ser182 residue of SrLDC and the corresponding residues in other O/LDCs are shown as stick models and labeled. Hydrogen bonds between the serine residue and the phosphate moiety of PLP are shown as red-colored dotted lines.

(TIF)

S3 Fig. Contacts of VvL/ODC with neighboring molecules. One VvL/ODC structure is shown as a cartoon diagram. The AS-loop, the PS-loop and the R-loop of VvL/ODC are colored orange, cyan, and magenta, respectively. The molecules near VvL/ODC are shown as surface models with different colors.

(TIF)

Acknowledgments

This work was supported by a National Research Foundation of Korea (NRF) grant (NRF-2014M1A2A2033626) and by C1 Gas Refinery Program through the National Research Foundation of Korea (NRF) funded by the Ministry of Science, ICT & Future Planning (NRF-2016M3D3A1A01913269), and was also supported by the New & Renewable Energy Core Technology Program of the Korea Institute of Energy Technology Evaluation and Planning (KETEP) granted financial resource from the Ministry of Trade, Industry & Energy, Republic of Korea (20153030091360).

Author Contributions

Conceptualization: KJK YHK ILK.

Investigation: HYS HFS SHK.

Supervision: KJK.

Writing – original draft: HYS KJK.

References

1. Tabor CW, Tabor H. Polyamines in microorganisms. *Microbiological reviews*. 1985; 49(1):81. PMID: [3157043](#)
2. Boeker EA, Snell EE. 7 Amino Acid Decarboxylases. *The enzymes*. 1972; 6:217–53.
3. Richard H, Foster JW. *Escherichia coli* glutamate- and arginine-dependent acid resistance systems increase internal pH and reverse transmembrane potential. *Journal of bacteriology*. 2004; 186(18):6032–41. doi: [10.1128/JB.186.18.6032-6041.2004](#) PMID: [15342572](#)
4. Castanie-Cornet M-P, Penfound TA, Smith D, Elliott JF, Foster JW. Control of acid resistance in *Escherichia coli*. *Journal of Bacteriology*. 1999; 181(11):3525–35. PMID: [10348866](#)
5. Bearson S, Bearson B, Foster JW. Acid stress responses in enterobacteria. *FEMS microbiology letters*. 1997; 147(2):173–80. PMID: [9119190](#)
6. Park YK, Bearson B, Bang SH, Bang IS, Foster JW. Internal pH crisis, lysine decarboxylase and the acid tolerance response of *Salmonella typhimurium*. *Molecular microbiology*. 1996; 20(3):605–11. PMID: [8736539](#)

7. Neely MN, Olson ER. Kinetics of expression of the *Escherichia coli* cad operon as a function of pH and lysine. *Journal of bacteriology*. 1996; 178(18):5522–8. PMID: [8808945](#)
8. Brickman TJ, Armstrong SK. The ornithine decarboxylase gene *odc* is required for alcaligin siderophore biosynthesis in *Bordetella* spp.: putrescine is a precursor of alcaligin. *Journal of bacteriology*. 1996; 178(1):54–60. PMID: [8550442](#)
9. Sturgill G, Rather PN. Evidence that putrescine acts as an extracellular signal required for swarming in *Proteus mirabilis*. *Molecular microbiology*. 2004; 51(2):437–46. doi: [10.1046/j.1365-2958.2003.03835.x](#) PMID: [14756784](#)
10. Patel CN, Wortham BW, Lines JL, Fetherston JD, Perry RD, Oliveira MA. Polyamines are essential for the formation of plague biofilm. *Journal of bacteriology*. 2006; 188(7):2355–63. doi: [10.1128/JB.188.7.2355-2363.2006](#) PMID: [16547021](#)
11. Schneider J, Wendisch VF. Biotechnological production of polyamines by bacteria: recent achievements and future perspectives. *Applied microbiology and biotechnology*. 2011; 91(1):17–30. doi: [10.1007/s00253-011-3252-0](#) PMID: [21552989](#)
12. Platt DK. Engineering and high performance plastics market report: a Rapra market report: iSmithers Rapra Publishing; 2003.
13. Willke T, Vorlop KD. Industrial bioconversion of renewable resources as an alternative to conventional chemistry. *Appl Microbiol Biotechnol*. 2004; 66(2):131–42. doi: [10.1007/s00253-004-1733-0](#) PMID: [15372215](#).
14. Flieger M, Kantorova M, Prell A, Řezanka T, Votruba J. Biodegradable plastics from renewable sources. *Folia microbiologica*. 2003; 48(1):27–44. PMID: [12744074](#)
15. Mimizuka T, Kazami J, inventorsHost and method for producing cadaverine2002.
16. Nishi K, Endo S, Mori Y, Totsuka K, Hirao Y. Method for producing cadaverine dicarboxylate. Google Patents; 2007.
17. Mimitsuka T, Sawai H, Hatsu M, Yamada K. Metabolic engineering of *Corynebacterium glutamicum* for cadaverine fermentation. *Bioscience, biotechnology, and biochemistry*. 2007; 71(9):2130–5. doi: [10.1271/bbb.60699](#) PMID: [17895539](#)
18. Tateno T, Okada Y, Tsuchidate T, Tanaka T, Fukuda H, Kondo A. Direct production of cadaverine from soluble starch using *Corynebacterium glutamicum* coexpressing α -amylase and lysine decarboxylase. *Applied microbiology and biotechnology*. 2009; 82(1):115–21. doi: [10.1007/s00253-008-1751-4](#) PMID: [18989633](#)
19. Kind S, Jeong WK, Schröder H, Wittmann C. Systems-wide metabolic pathway engineering in *Corynebacterium glutamicum* for bio-based production of diaminopentane. *Metabolic engineering*. 2010; 12(4):341–51. doi: [10.1016/j.ymben.2010.03.005](#) PMID: [20381632](#)
20. Qian ZG, Xia XX, Lee SY. Metabolic engineering of *Escherichia coli* for the production of cadaverine: a five carbon diamine. *Biotechnology and bioengineering*. 2011; 108(1):93–103. doi: [10.1002/bit.22918](#) PMID: [20812259](#)
21. Lee JW, Kim HU, Choi S, Yi J, Lee SY. Microbial production of building block chemicals and polymers. *Current opinion in biotechnology*. 2011; 22(6):758–67. doi: [10.1016/j.copbio.2011.02.011](#) PMID: [21420291](#)
22. Nishi K, Endo S, Mori Y, Totsuka K, Hirao Y. Method for producing cadaverine dicarboxylate and its use for the production of nylon. European Patent: EP1482055 (B1). 2006.
23. Ma W, Cao W, Zhang B, Chen K, Liu Q, Li Y, et al. Engineering a pyridoxal 5'-phosphate supply for cadaverine production by using *Escherichia coli* whole-cell biocatalysis. *Scientific reports*. 2015; 5.
24. Otwinowski Z, Minor W. [20] Processing of X-ray diffraction data collected in oscillation mode. *Methods in enzymology*. 1997; 276:307–26.
25. Matthews BW. Solvent content of protein crystals. *Journal of molecular biology*. 1968; 33(2):491–7. PMID: [5700707](#)
26. Vagin A, Teplyakov A. Molecular replacement with MOLREP. *Acta Crystallographica Section D: Biological Crystallography*. 2009; 66(1):22–5.
27. Emsley P, Cowtan K. Coot: model-building tools for molecular graphics. *Acta Crystallographica Section D: Biological Crystallography*. 2004; 60(12):2126–32.
28. Murshudov GN, Vagin AA, Dodson EJ. Refinement of macromolecular structures by the maximum-likelihood method. *Acta Crystallographica Section D: Biological Crystallography*. 1997; 53(3):240–55.
29. Krissinel E, Henrick K. Inference of macromolecular assemblies from crystalline state. *Journal of molecular biology*. 2007; 372(3):774–97. doi: [10.1016/j.jmb.2007.05.022](#) PMID: [17681537](#)

30. Almrud JJ, Oliveira MA, Kern AD, Grishin NV, Phillips MA, Hackert ML. Crystal structure of human ornithine decarboxylase at 2.1 Å resolution: structural insights to antizyme binding. *Journal of molecular biology*. 2000; 295(1):7–16. doi: [10.1006/jmbi.1999.3331](https://doi.org/10.1006/jmbi.1999.3331) PMID: [10623504](https://pubmed.ncbi.nlm.nih.gov/10623504/)
31. Shah R, Akella R, Goldsmith EJ, Phillips MA. X-ray structure of Paramecium bursaria chlorella virus arginine decarboxylase: insight into the structural basis for substrate specificity. *Biochemistry*. 2007; 46(10):2831–41. doi: [10.1021/bi6023447](https://doi.org/10.1021/bi6023447) PMID: [17305368](https://pubmed.ncbi.nlm.nih.gov/17305368/)
32. Balk H, Merkl I, Bartholmes P. Circular dichroism studies on the interaction of tryptophan synthase with pyridoxal 5'-phosphate. *Biochemistry*. 1981; 20(22):6391–5. PMID: [7030390](https://pubmed.ncbi.nlm.nih.gov/7030390/)
33. Lee SG, Hong SP, Kim DY, Song JJ, Ro HS, Sung MH. Inactivation of tyrosine phenol-lyase by Pictet–Spengler reaction and alleviation by T15A mutation on intertwined N-terminal arm. *FEBS Journal*. 2006; 273(24):5564–73. doi: [10.1111/j.1742-4658.2006.05546.x](https://doi.org/10.1111/j.1742-4658.2006.05546.x) PMID: [17094783](https://pubmed.ncbi.nlm.nih.gov/17094783/)
34. Percudani R, Peracchi A. A genomic overview of pyridoxal-phosphate-dependent enzymes. *EMBO reports*. 2003; 4(9):850–4. doi: [10.1038/sj.embor.embor914](https://doi.org/10.1038/sj.embor.embor914) PMID: [12949584](https://pubmed.ncbi.nlm.nih.gov/12949584/)
35. Kim HJ, Kim YH, Shin J-H, Bhatia SK, Sathiyarayanan G, Seo H-M, et al. Optimization of Direct Lysine Decarboxylase Biotransformation for Cadaverine Production with Whole-Cell Biocatalysts at High Lysine Concentration. *J Microbiol Biotechnol*. 2015; 25(7):1108–13. doi: [10.4014/jmb.1412.12052](https://doi.org/10.4014/jmb.1412.12052) PMID: [25674800](https://pubmed.ncbi.nlm.nih.gov/25674800/)